Developmental Biology 526 (2025) 1–14

Contents lists available at ScienceDirect

Developmental Biology

journal homepage: www.elsevier.com/locate/developmentalbiology

Original research article

Calreticulin is required for cuticle deposition and trabeculae formation inside butterfly wing scale cells

Ru Hong *, Cédric Finet, Antónia Monteiro **

Department of Biological Sciences, National University of Singapore, Singapore, Singapore

A B S T R A C T

Insect cuticle is normally deposited outside the plasma membrane of epidermal cells, making it unclear how cuticular pillars (trabeculae) are found inside butterfly wing scale cells. By co-labelling the cuticle and the plasma membrane, we found evidence that the plasma membrane invaginates towards the interior of the scale during development, and that chitin pillars form within these invaginations within the cell, but topologically outside it. Furthermore, we found that Calreticulin, a multifunctional protein, is essential for the formation of these trabeculae. The signal from an antibody targeting this protein was found colocalized with chitin outside the cell membrane, as scales were developing, and a *calreticulin* gene knockout led to loss of chitin pillars, disruption of other scale morphologies, and loss of pigmentation. Our results implicate this multifunctional protein in butterfly wing scale coloration and morphology.

1. Introduction

One of the characteristics of butterflies and moths is their colorful and complex wing scales. These scales can contain pigments (Giraldo and Stavenga, 2008; Zhang et al., 2017; Matsuoka and Monteiro, 2018; Forman and Thulin, 2022) and can be sculpted in elaborate ways to reflect brilliant colors (Ghiradella, 1991; Vukusic and Sambles, 2003, Nishida et al., 2023, Finet et al., 2024). Each scale is the dried cuticular skeleton of a scale cell and this skeleton contains chitin, an N-acetyl-glucosamine polymer produced by chitin synthase, an enzyme normally attached to the plasma membrane of cells (Klowden, 2013; Dinwiddie et al., 2014; Day et al., 2019; Nakazato and Otaki, 2023a). The scale grows outward during the pupal stage of development. Newly grown-out scales look like baseball bats, but they gradually flatten into wider and thinner paddle-like structures (Dinwiddie et al., 2014; McDougal et al., 2021; Lloyd et al., 2024). When scale development is completed, just before adult eclosion, scale cells die leaving behind their cuticle skeleton.

The archetypal skeleton of a butterfly scale is composed of the upper surface, which is mainly assembled from a grid of longitudinal ridges and transverse crossribs, a lower lamina, and pillar-like trabeculae, which connect the upper surface to the lower lamina (Ghiradella and Radigan, 1976). In some species, the lumen of the scale is filled with cuticle with more complex and elaborate morphologies. For example, colorful scales of some Papilionidae show a honeycomb lattice between ridges on the upper surface, and some Lycaenidae have perforated multilayer lattices attached to their lower lamina (Ghiradella and Radigan, 1976; Ghiradella, 1984; Ghiradella, 1985; Prum et al., 2006; Seah and Saranathan, 2023). What is unique about scales, relative to other types of insect cuticles, is that these cuticular structures are found inside (in the lumen) of dead scale cells, while cuticle is usually deposited to the outside of the plasma membrane of cells (Binnington and Retnakaran, 1991; Merzendorfer and Zimoch, 2003; Merzendorfer, 2006; Klowden, 2013, Sobala et al., 2015, Zhu et al., 2016, Liu et al., 2019).

Early electron microscopy observations of *Colias eurytheme* and *Mitoura grynea* butterfly pupal wings revealed a close association between cellular membranes and cuticle deposition within the lumen of scale cells, which exhibited a pillar-like and complex gyroid-shaped cuticular skeleton, respectively (Ghiradella, 1974, 1989). Based on these findings, Ghiradella proposed that trabeculae formation was linked to the invagination of the plasma membrane. Transmission electron microscopy (TEM) images of *Mitoura grynea* pupal wing scales showed dense crystallite-like structures, surrounded by two membranes, interpreted as the plasma membrane (PM) and the smooth endoplasmic reticulum (SER) membrane (Ghiradella, 1989). This led to the development of a chitin deposition model, suggesting that the SER, by budding off from the endoplasmic reticulum (ER), facilitated the invagination and scaffolding of the PM into the cell lumen, enabling the secretion of the gyroid cuticular skeleton (Ghiradella, 1989). This model, however, has not been validated as no PM nor SER markers were used to distinguish these cellular membranes or to identify the position of these membranes relative to cuticle deposition.

* Corresponding author.
** Corresponding author.
E-mail addresses: rhong001@e.ntu.edu.sg (R. Hong), antonia.monteiro@nus.edu.sg (A. Monteiro).

https://doi.org/10.1016/j.ydbio.2025.06.013
Received 3 November 2024; Received in revised form 16 June 2025; Accepted 17 June 2025
Available online 18 June 2025

Different visualization techniques have been applied to study the morphogenesis of scales. Traditionally, pupal wings are dissected and fixed at different developmental time points, and visualized with electron microscopy (EM) and confocal imaging (Ghiradella, 1989, Ghiradella, 1994, Dinwiddie et al., 2014; Day et al., 2019; Seah and Saranathan, 2023, Lloyd et al., 2024). More recently, real-time in vivo imaging technology was adopted to further explore scale development (Iwata et al., 2014; Hirata and Otaki, 2019, McDougal et al., 2021; Nakazato and Otaki, 2023a,b). However, the limited resolution of conventional confocal fluorescence microscopes and the accumulation of dense cuticle, as well as the lack of adequate stains in EM imaging, have hampered a detailed understanding of scale development. To date, thus, the process of how a stereotypical scale forms, how cuticle gets to be deposited on the inside of a scale cell to form simple trabeculae, and which proteins participate in this process, are still unresolved.

To understand how cuticle is being deposited inside a scale cell, we performed immunofluorescence on ultrathin sections of *Bicyclus anynana* butterfly wings, whose scales have an archetypal structure: with cuticular pillars traversing the lumen of the scale from top to bottom. We imaged these scales with a super-resolution microscope to colocalize the plasma membrane and chitin, the main component of the insect cuticle. Using immunogold labeling, we found that either Calreticulin, an ER resident multifunctional protein, or Calnexin, a paralog, were located outside the scale cell membrane and within the cuticular matrix. A CRISPR knockout revealed that Calreticulin is required for the formation of trabeculae, crossribs, and other scale nanostructures. Our work discovered an essential role of Calreticulin in scale cuticle structure development.

2. Results

2.1. Anti-Calreticulin signal colocalizes with chitin in B. anynana wing scales

Complex membrane-cuticle lattice structures are forming around 70 % of pupal development (Ghiradella, 1989). Thus, we selected 120-h and 136-h after pupa formation (APF) (77 and 88 % development, respectively) to investigate trabeculae formation in *B. anynana* wing scales. An antibody against the classic ER marker Calreticulin (Moretti et al., 2017; de la Roche et al., 2018; Wan et al., 2020; Wang et al., 2022), generated using full-length recombinant human CALRETICULIN as the immunogen, was then used in an immunogold labeling reaction (Fig. 1A–A’’’).

To validate the specificity of the antibody, a Western blot analysis was performed following the instructions described in (Choi et al., 2002). The result revealed two distinct bands (Fig. S1A). One of the bands appears at approximately 50 kDa (Fig. S1A, red arrow), which corresponds to the expected molecular weight of Calreticulin protein detected using this antibody. However, an additional band is observed at approximately 75 kDa (Fig. S1A, blue arrow), which is likely attributable to Calnexin, a paralog from the same gene family (Schrag et al., 2001). Blastp analysis comparing human Calreticulin against the *B. anynana* proteome revealed that Calreticulin exhibits the highest sequence similarity, whereas Calnexin shares comparatively lower similarity (Fig. S1B).

The anti-Calreticulin signal showed clear colocalization with the cuticular matrix of wing scales, as the gold particles were found inside ridges, crossribs, trabeculae, and upper and lower laminae in both 120-h (Fig. 1B–B’’’) and 136-h APF wing scales (Fig. 1C–C’’’). This suggests that Calreticulin may be located outside the ER and outside the scale cell membrane.

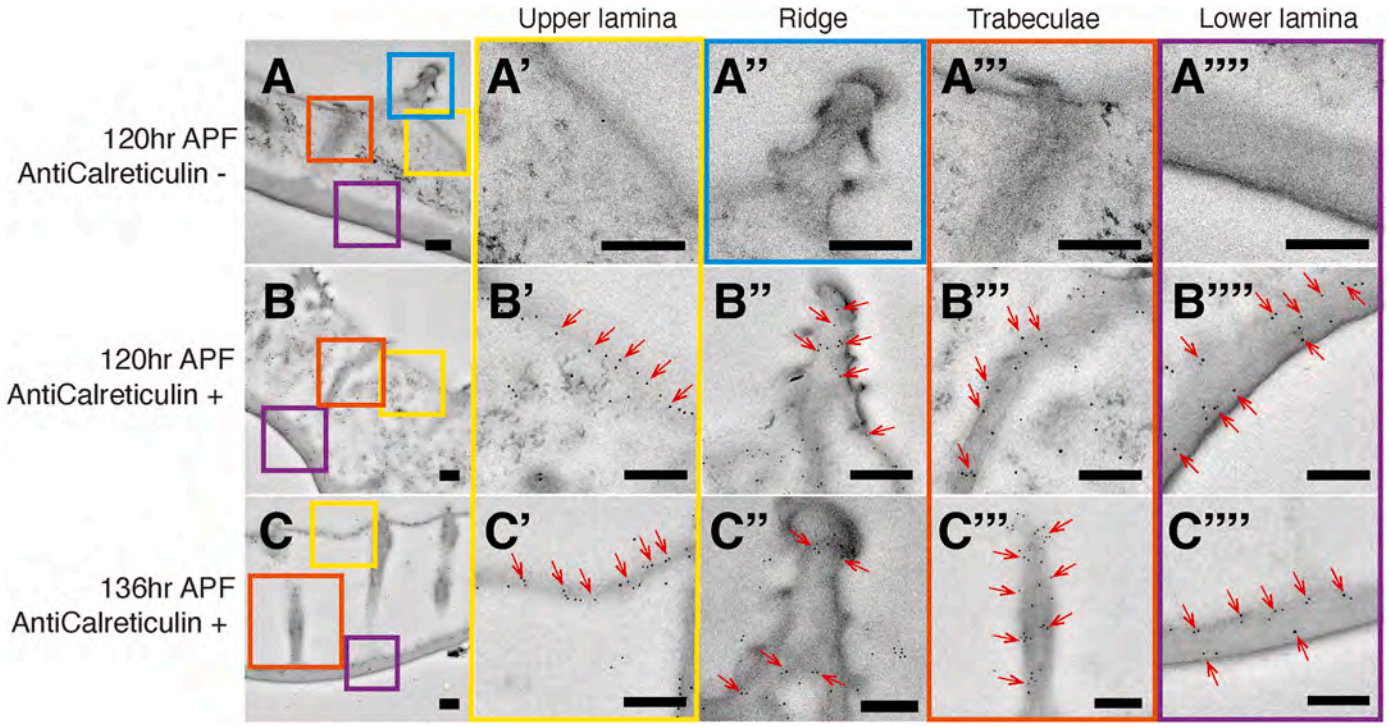

Fig. 1. Anti-Calreticulin signal is localized in the cuticular matrix, both on the surface and inside scale cells of *B. anynana*. (A-A’’’’) Immunogold negative control staining on a 120-h APF pupal wing section. Immunogold staining of Calreticulin on a 120-h APF wing section (B-B’’’’) and a 136-h APF wing section (C-C’’’’). Colloidal gold size: 5 nm. Enlarged view of different ultra-structures: upper lamina (A’-C’); ridge (A’’-C’’); trabecula (A’’’-C’’’); lower lamina (A’’’’-C’’’’). Red arrows indicate the immunogold particles. Scale bars: 200 nm. (For interpretation of the references to color in this figure legend, the reader is referred to the Web version of this article.)

2.2. Chitin and the anti-Calreticulin signal appear to be topologically localized outside the scale cell

To colocalize the PM and the cuticular matrix, we used immunofluorescence on ultrathin resin-embedded wing sections. We used a house-made antibody against *B. anynana* Armadillo (Banerjee et al., 2023) to visualize the PM, and Wheat Germ Agglutinin (WGA) conjugated with a fluorescent marker to visualize the cuticular matrix. WGA is commonly used to stain chitin (Dinwiddie et al., 2014; Seah and Saranathan, 2023), a core component of the cuticular matrix, and Armadillo, known as β-Catenin in Drosophila, though involved in the Wnt signaling pathway in the cytoplasm, is often also localized on the plasma membrane (Peifer et al., 1994; Cox et al., 1996), including in butterfly wings scales (Dinwiddie et al., 2014; Banerjee and Monteiro, 2020), and has been previously used as a marker for the apical cell membrane in an insect chitin deposition study (De Giorgio et al., 2023). The tissue sections were first examined under a conventional confocal microscope, but the resolution of these images did not allow us to distinguish the localization of chitin and cell membranes. However, Armadillo did show a positive signal in the scale cells, compared with the negative control preparation, where the antibody against Armadillo was left out (Fig. 2A and B). We then switched to STED super-resolution microscopy (Hell and Wichmann, 1994) to improve image resolution. Despite some background noise, the visualization of chitin was clear: WGA stained the typical scale cuticular nanostructures, such as ridges and upper and lower laminae (Fig. 2C–C'''). Armadillo signals were visible throughout the interior of the scale cross sections (Fig. 2C–C'''), and sometimes right next to (and around) chitin that was being deposited on the inside (but topologically on the outside) of a scale cell (Fig. 2C', pink and blue arrowheads). Consistent with this labeling, a structure resembling PM

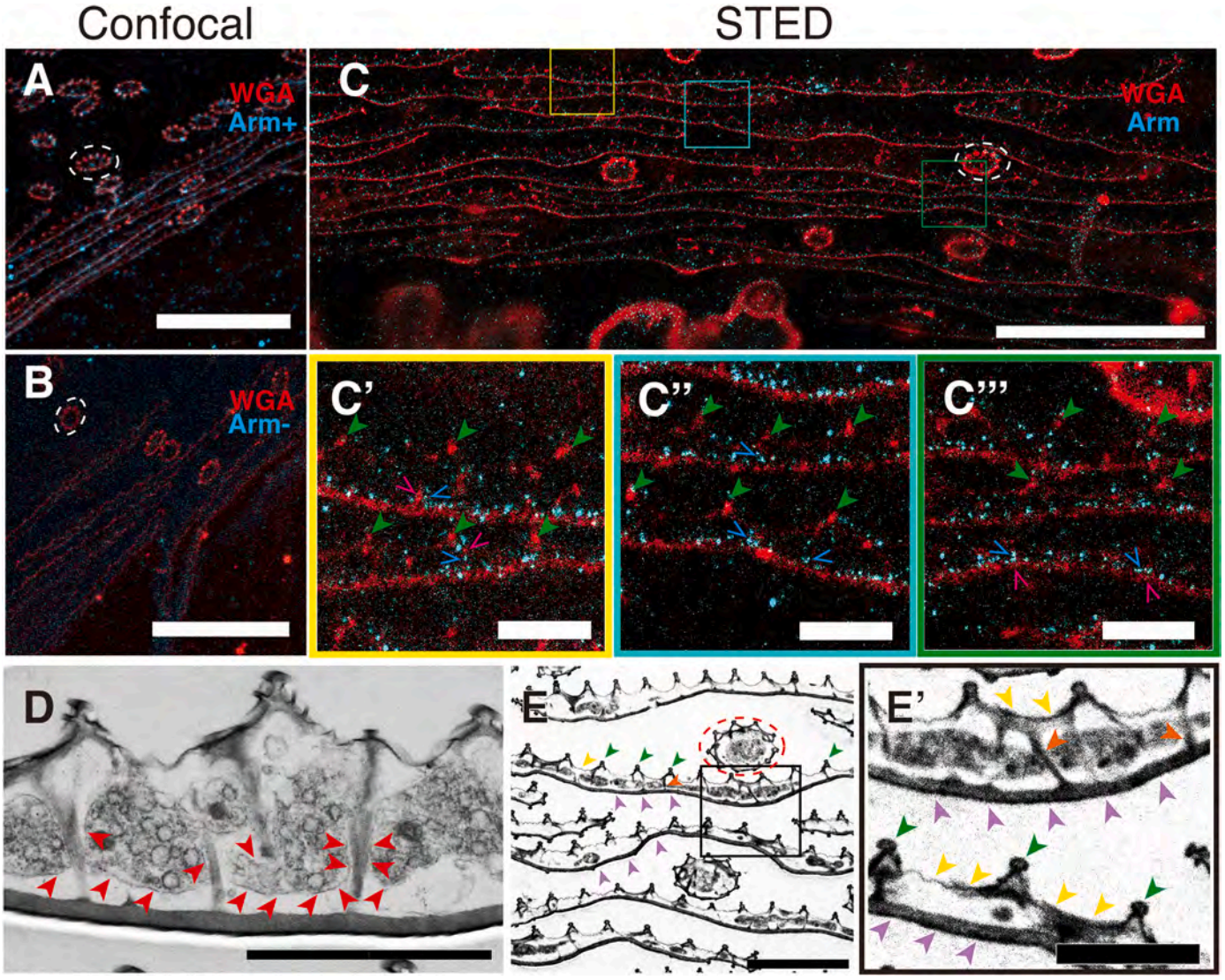

Fig. 2. Chitin fingers (WGA staining) are found on the interior of brown scale cells often surrounded by plasma membrane (Arm staining). (A) Confocal image of Armadillo and WGA immunostainings on a *B. anynana* 136-h APF wing section. (B) A negative control lacking the primary antibody against Armadillo. (C-C''') STED super-resolution images of Armadillo and WGA. (C'-C''') Enlarged-view images of the regions highlighted in (C). Green arrowheads indicate ridges. Blue arrowheads: Armadillo functions as a plasma membrane marker that surrounds or is tightly associated with WGA-labeled chitin (Pink arrowheads) in vertical trabecula-like structures that are contiguous with the chitin on the outside of the cell (C'), and present across the lumen of scales (C''), and along the lower lamina (C'''). The single-channel views of (C-C''') are shown in Fig. S2. (D) Cross-sectional TEM image of a 131-h APF wing section. Red arrowheads indicate a plasma membrane-like structure. A sectional TEM image (E) and the enlarged-view image (E') of the black-squared region serve as schematic images of a cross-section view of a butterfly wing. Green arrowheads indicate ridges. Yellow arrowheads indicate upper laminae. Purple arrowheads indicate lower laminae. Orange arrowheads indicate trabeculae. The white dash circles in (A–C) and the red dash circles in (E) indicate scale stems. Scale bars: (A–C): 20 μm. (C′-C''', D, E'): 2 μm. (E): 5 μm. (For interpretation of the references to color in this figure legend, the reader is referred to the Web version of this article.)

was identified in 131-h APF wing sections stained with lead citrate under cross-sectional TEM. This membrane surrounded the trabeculae on both sides (Fig. 2D).

2.3. Knockout of calreticulin impacts pigmentation and scale morphology of brown and black scales

As the anti-Calreticulin signal was found in the cuticular matrix, we decided to test the function of Calreticulin in scale development. We

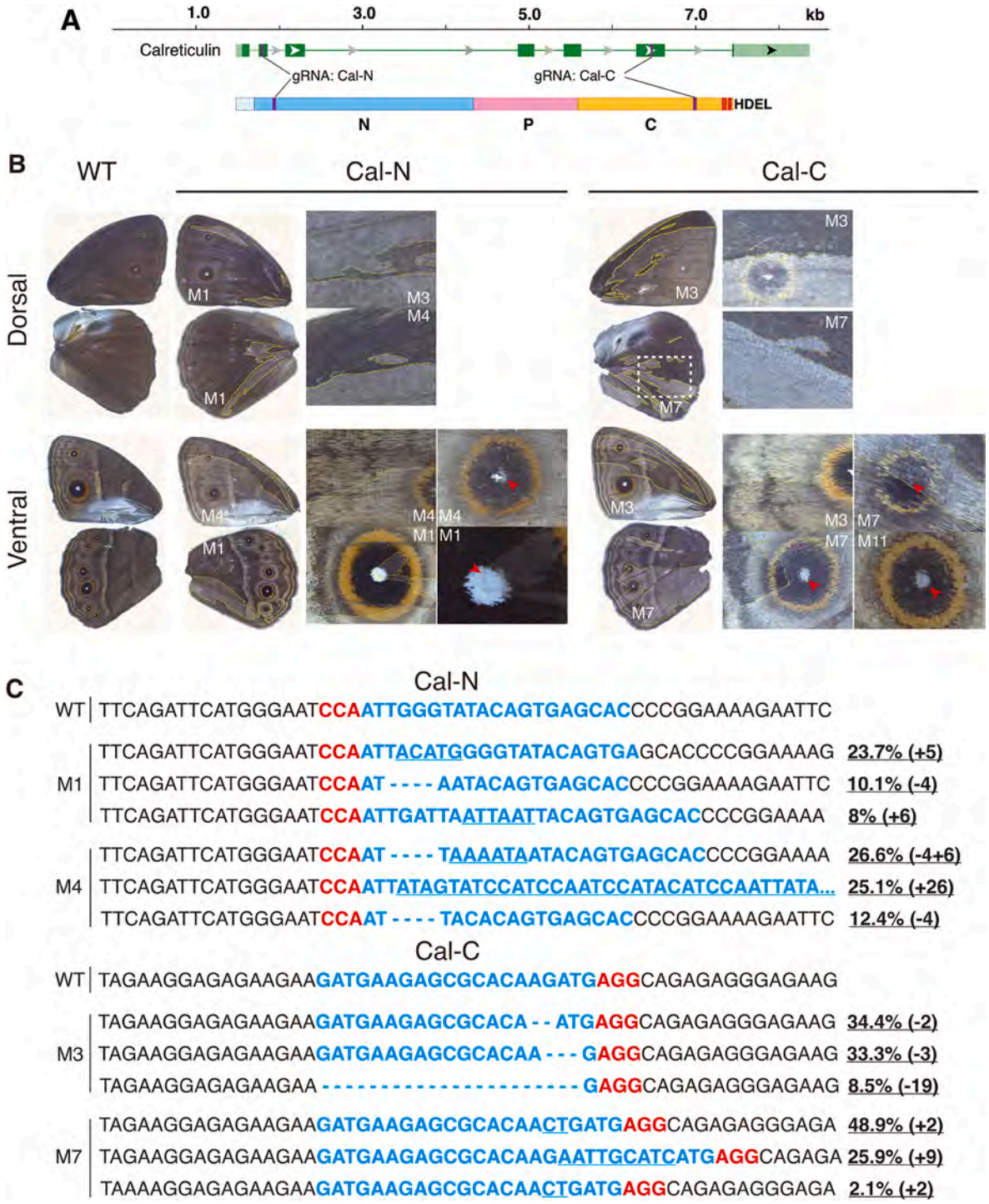

Fig. 3. *calreticulin* gene structure and mosaic crispants show loss of melanin pigmentation and partial loss of white scales in the eyespot centers of *B. anynana*. (A) Schematic of *B. anynana calreticulin* gene and encoded protein. N, P and C indicate the N-, P-, and C-domains of Calreticulin. HDEL indicates the motif which prevents secretion from ER. Guide RNA targeting sites are shown in purple. Red bars indicate motifs which are highly conserved across Lepidoptera. (B) Left column: a wildtype (WT) male *B. anynana* dorsal and ventral side views. Middle column: Cal-N crispants. Higher magnification images show color change of scales in mutant wing areas. Right column: Cal-C crispants. Both Cal-N and Cal-C crispants show loss of eyespot center white scales (red arrowheads). The white dashed rectangle indicates an example of a wing patch collected for genotyping. (C) The top three most abundant indel alleles in the wings of two representative mutants for each guide RNA. Blue indicates the regions targeted by the guide RNA. Red indicates the protospacer adjacent motifs (PAM). Hyphens indicate deletions. Underlined bases indicate insertions. (For interpretation of the references to color in this figure legend, the reader is referred to the Web version of this article.)

designed a single guide RNA (sgRNA) to target the N-terminus of the transcript using CRISPR-Cas9 (Cal-N, Fig. 3A, Fig. S3). Considering that this protein is indispensable for embryonic development (Michalak et al., 2009), another sgRNA was designed to disrupt the C-terminal domain (Cal-C, Fig. 3A, Fig. S3), as frame-shifting mutations in this domain lead to the survival of human cells (Klampfl et al., 2013; Nangalia et al., 2013; Pietra et al., 2016).

Both guides led to similar mutant phenotypes but had different success rates. As expected, embryos injected with Cal-N targeting the N-terminus were mostly inviable: among the 251 larvae that hatched (hatching rate: 43.4 %), only 10 larvae survived till adulthood (eclosion rate: 4 %). Of those adults, five (50 %) showed mosaic phenotypes (Fig. 3B, Fig. S4). Survival was higher with Cal-C targeting the C-terminal domain: among the 162 hatched larvae (hatching rate: 45.9 %), 36 eclosed into butterflies (eclosion rate: 22 %), and 23 showed mosaic phenotypes (64 %) (Fig. 3B, Fig. S4). Both Cal-N and Cal-C crispants exhibited paler scales on both dorsal and ventral sides of wings, regardless of sex (female versus male: Cal-N:1:3, Cal-C: 10: 13, Fig. 3B, Fig. S4), with less defined crossribs, whereas most of the white scales in the eyespot centers were missing (Fig. 3B). Next-generation sequencing (NGS) of the affected wing tissue from some of these mosaic mutants confirmed that *calreticulin* was targeted at the two expected gene locations (Fig. 3C, Supplementary data- Cal Mutant genotype.xlsx). With one exception (Cal-N M3, with 21.9 % reads causing frameshifts), the frequency of indels causing frameshifts was larger than 50 % (ranging from 22 to 93 %; Table 1), suggesting that these mutant wings resulted from either homozygous or hemizygous mutations which contained two different mutated alleles (Table 1, Supplementary data- Cal Mutant genotype.xlsx).

To quantify the color changes observed in the two types of crispants, we sampled and examined WT and knockout (mKO) scales from mutant individual #4 obtained from Cal-N CRISPR (Cal-N M4) and individual #7 obtained from Cal-C CRISPR (Cal-C M7). We first carried out absorbance measurements in both cover and ground scales from three different colored regions of the wing: dorsal brown scales, ventral brown scales, and ventral eyespot black scales. Almost all mKO scales showed a decrease in absorbance relative to WT scales sampled from the same region (Fig. S5A''-F'', Fig. S6A''-F''), (Table S2 xlsx). However, the absorbance spectrum curves did not change in shape, indicating that the mKO scales contained a similar pigment composition. Optical microscopy images confirmed these findings (Fig. S5A-F, A'-F', Fig. S6A-F, A'-F'). Mutations in the C- or N- terminal end of the gene produced similar phenotypes (Fig. S5, Fig. S6A-F''), suggesting that in both cases, Calreticulin's function in scale coloration was impaired similarly. Furthermore, we estimated a lower concentration of pigments in KO dorsal brown scales compared to WT, by calculating the absorption coefficient spectra of these scales from transmittance and lower lamina thickness measurements (Balakrishnan et al., 2023b) to quantify pigment concentration in the cuticle (Fig. S5A''', B''').

To investigate whether mKO scales were impaired in their morphology, we used SEM to examine the scale's surface, top-down TEM (Balakrishnan et al., 2023a) to view the scale's internal structure from the top, and FIB-SEM to obtain a cross-section of the scales. Strikingly, the crossrib morphology, which has a typical grid pattern in WT scales (Fig. 4A–A''), was significantly altered in mKO scales, forming a beaded-bracelet shape between ridges (Fig. 4B–B'', Fig. S6G and H) or becoming more irregular (Fig. 4B, Fig. S6G and H). Also, unlike WT scales, where open windows are found between the ridges and cross-ridges (Fig. 4A–A''), most of the mutant scales had their windows closed or half-closed with a thin cuticular film (Fig. 4B–B'', Fig. S6G and H). These changes were observed in both Cal-N M4 and Cal-C M7 mutants. Trabeculae in the mKO scales were also shorter or missing, resulting in the upper surface structures (ridges, crossribs, and window-covering film) becoming attached to the lower lamina in places (Fig. 4B''). These consistent color and morphological changes were not observed in other previous CRISPR knockout experiments targeting *B. anynana* genes, suggesting specificity of the guide RNAs and few off-target effects (Prakash and Monteiro, 2018, Prakash et al., 2022; Tian et al., 2024).

To quantify the structural changes in both cover and ground scales, we measured the height of ridges, crossribs, and trabeculae, the thickness of the lower lamina, and the distance between adjacent crossribs and ridges (Fig. 4A'', Fig. S7). We found that crossrib height (Fig. 4C) (p-value: cover scale = 6.77e-05; ground scale <2e-16) and trabecula height (Fig. 4E) (p-value: cover scale <2e-16; ground scale <2e-16) were significantly shorter in the mKO scales, as was the distance between adjacent crossribs (p-value: cover scale <2e-16; ground scale <2e-16) (Fig. 4D), whereas the other scale parameters were largely unchanged in either cover scales or ground scales (Fig. S7).

2.4. *Calreticulin knockout does not visibly affect the color of orange, white, and silver scales but alters the morphology of orange and white scales*

We subsequently investigated changes in the color and nanomorphology of three other scale types. Orange scales are found in the outer rings of the eyespots, silver scales are found in male androconial patches around the scent glands (Prakash et al., 2022), and white scales are found in the center of the eyespots, most of which disappeared altogether in *calreticulin* mutants (Fig. 3B).

The orange and silver scales did not appear to have changed in color after *calreticulin* disruption (Fig. S8D–G'', Fig. 5E–E'', Fig. S4, Table S2 xlsx). However, SEM and TEM images showed that mutant orange scales changed in morphology similarly to brown scales (Fig. S8A–C'), whereas silver scales showed no visible morphological or color changes in any of the mutants obtained in this study (Fig. 5E–E'', Fig. S4). Genetic data showed that silver scales in one of the Cal-N M4 forewings were genetically altered for *calreticulin* with a frame-shifting indel frequency

Table 1
Summary of mutant allele reads at the calreticulin loci targeted by the two guides. Cal-N M4S indicates the genomic DNA sample extracted from the silver area of a Cal-N M4 forewing. Sequencing details can be found in Supplementary data- Cal Mutant genotype.xlsx.

samples	Total reads	Non-frameshifting reads	Frameshifting reads	% reads causing non-frameshifts	% reads causing frameshifts
Cal-N M1	8043	2612	5431	32.5 %	67.5 %
Cal-N M3	9341	7294	2047	78.1 %	21.9 %
Cal-N M4	8812	1306	7506	14.8 %	85.2 %
Cal-N M4S	9555	630	8925	6.6 %	93.4 %
Cal-C M1	8209	3105	5104	37.8 %	62.2 %
Cal-C M3	8443	4097	4346	48.5 %	51.5 %
Cal-C M7	11289	3969	7320	35.2 %	64.8 %
Cal-C M10	6184	990	5194	16.0 %	84.0 %
Cal-C M11	9579	1797	7782	18.8 %	81.2 %
Cal-C M12	8741	2021	6720	23.1 %	76.9 %
Cal-C M13	9444	4706	4738	49.8 %	50.2 %
Cal-C M14	8026	1535	6491	19.1 %	80.9 %
Cal-C M22	7664	1664	6000	21.7 %	78.3 %

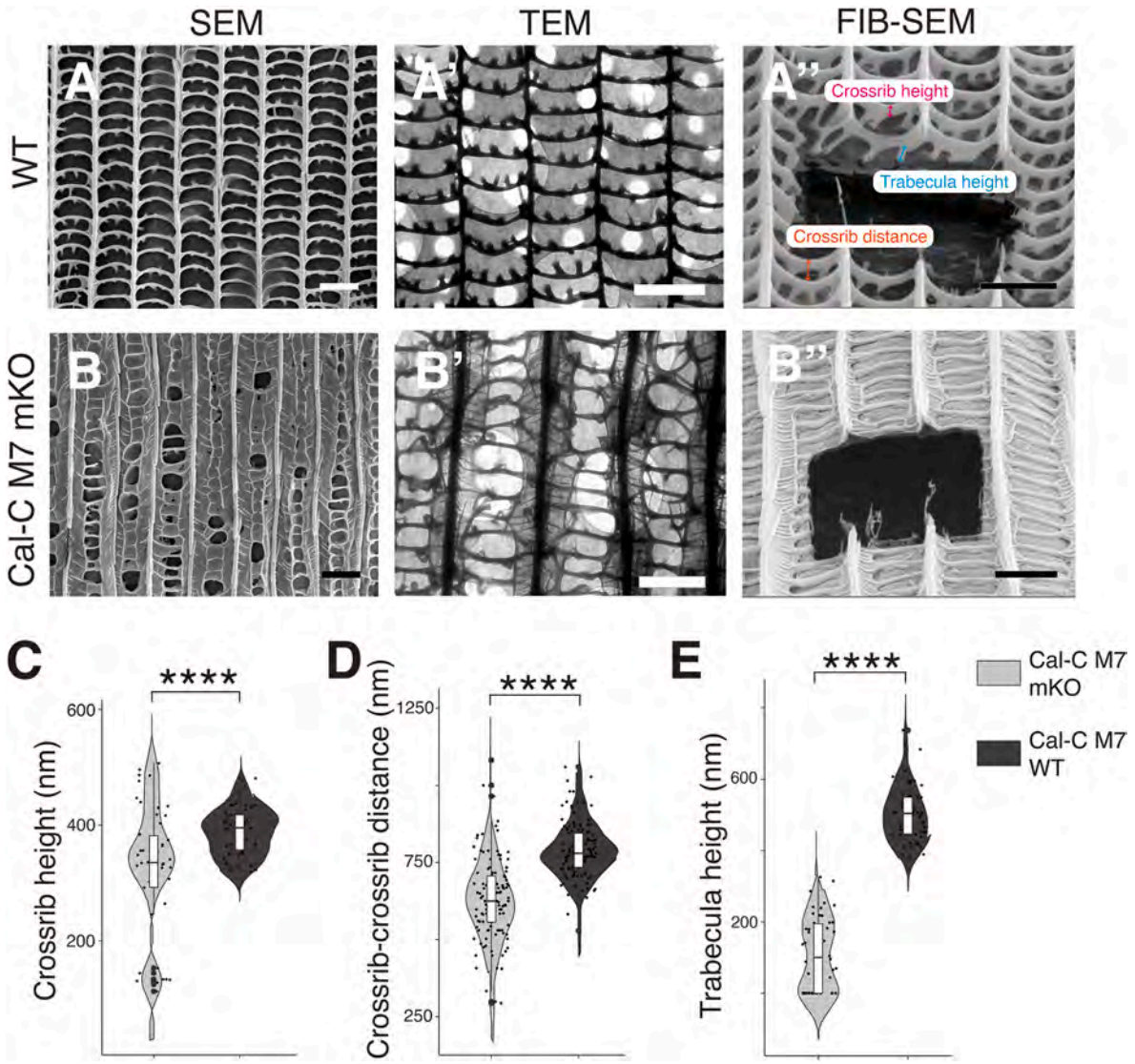

Fig. 4. *calreticulin* knockout causes morphological changes in brown cover scales. (A, B) SEM images of the WT and Cal-C M7 mKO dorsal brown scales. (A', B') Top-down TEM images. (A'', B'') FIB-SEM images of a cross-section of the scales. Scale bars: 2 μm. (C–E) Violin plots of Cal-C M7 cover scale crossrib and trabecula heights, and adjacent crossrib distance. Crossrib height and trabecula height: n = 5, measurements = 50, crossrib-crossrib distance: n = 5, measurements = 125. ****: $p < 0.0001$. The central line in the violin plot indicates the median of the distribution, while the top and bottom of the box represent the third and first quartiles of the data, respectively. The whiskers show up to 1.5 times the interquartile range. (For interpretation of the references to color in this figure legend, the reader is referred to the Web version of this article.)

of 93.4 % (Table 1) yet showed no significant changes relative to WT silver scales in overall appearance (Fig. 5A and B), morphology (Fig. 5C–C'', D-D''), or color (Fig. 5E–E''). FIB-SEM measurement analysis showed, however, that in Cal-N M4 mKO silver scales, the upper and lower laminae became thicker, and the ridge-ridge distance became wider (Fig. 5C'', D'', G-I). WT silver scales display unevenly distributed microribs on a closed upper lamina (Fig. 5C), instead of crossribs and open windows, as seen in all other colorful scales (Fig. 4A, Fig. S8A). They also have web-like trabeculae connecting the upper and lower surface instead of pillar-like trabeculae (Fig. 5C', C''). The key parameter that influences the reflectance of silver scales is the air layer thickness (Prakash et al., 2022), and this was not altered in Calreticulin knockouts (Fig. 5F), which explains why the appearance of these scales remained the same.

To investigate why white scales were affected by *calreticulin* mutations we used SEM and FIB-SEM to image their morphology in WT individuals (Fig. 6A) and in Cal-N M4 by picking residual white scales from the forewing eyespot centers (Figs. 3B and 6B). This type of scale has a grid-like upper surface nanostructure, similar to the colorful scales, but with a few more partially closed windows, and has long, irregular trabeculae projecting downwards from the crossribs (Fig. 6C–C'). Calreticulin knockouts led to disordered crossribs, pointing in all directions, making the distance between adjacent crossribs impossible to measure (Fig. 6D). In most areas, the scale lumen completely disappeared (Fig. 6D'), and the trabecula height was close to zero (Fig. 6F).

All these data indicate that *calreticulin* primarily impacts the development of scales that have well-defined crossribs, and associated trabeculae, such as white, orange, brown, and black scales, but not silver scales (Table 2).

Based on the Western blot analysis, we cannot completely rule out the possibility that Calnexin (in addition to, or instead of Calreticulin) is among the proteins colocalized with the cuticle. However, functional evidence derived from the Calreticulin knockout experiments provides compelling support for a critical role of Calreticulin in cuticle morphogenesis. This functional dependency strongly reinforces the interpretation that Calreticulin is indeed one of the proteins associated with

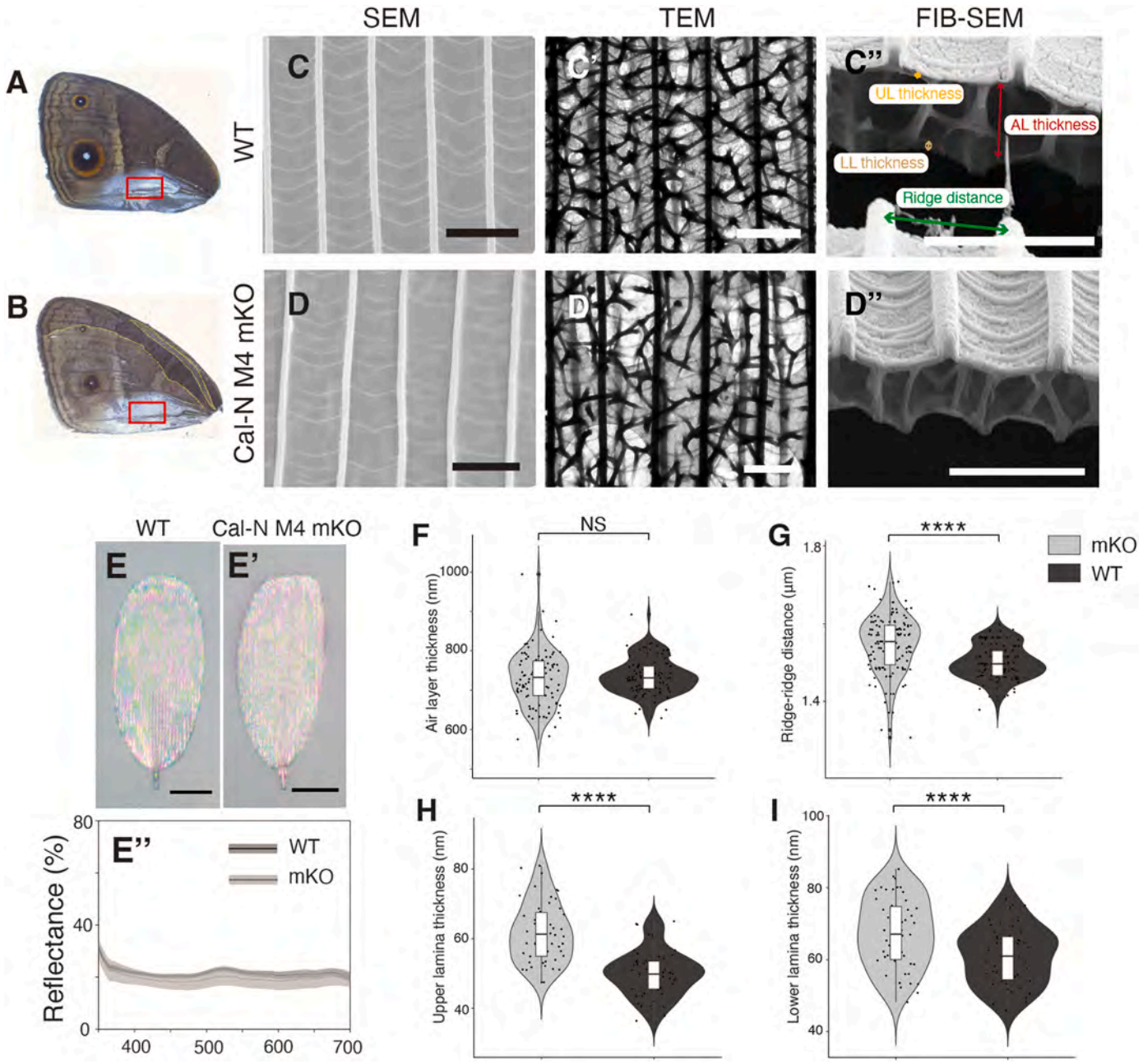

Fig. 5. Calreticulin knockouts cause slight alterations of silver scales, but reflectance spectra were not affected. SEM, TEM, FIB-SEM and optical microscopy images of WT (C-C'', E) and Cal-N M4 mKO silver scales (D-D'', E') taken from the red-rectangle demarcated areas in A and B, respectively. (E'') Reflectance spectra of the mKO silver scales exhibits similar patterns as WT. Scale bars: (C-D'') 2 μm, (E, E') 20 μm. (F–I) Violin plots of Cal-N M4 mKO and WT silver scales air layer (AL) thickness, upper and lower lamina thicknesses, and adjacent ridge-ridge distance. air layer thickness: n = 5, measurements = 100; upper and lower lamina thickness: n = 5, measurements = 50; adjacent ridge distance: n = 5, measurements = 125. ****: $p < 0.0001$, NS: not significant. The central line in the violin plot indicates the median of the distribution, while the top and bottom of the box represent the third and first quartiles of the data, respectively. The whiskers show up to 1.5 times the interquartile range. Tissue collected for genotyping is within the red rectangle. (For interpretation of the references to color in this figure legend, the reader is referred to the Web version of this article.)

cuticle, as observed in the immunogold labeling.

2.5. Lepidopteran Calreticulin

Guide RNA Cal-C only influenced a short sequence at the C-terminal end (Fig. S3). However, the phenotype it produced was similar to Cal-N crispants. To explain this result, we sought to identify motifs that could function in scale cuticular development at the C-terminal end of *B. anynana*. Only a single isoform of *calreticulin* was found in the *B. anynana* genome and transcriptome (Nowell et al., 2017; Saccheri et al., 2023). To compare the amino acid sequence of this protein to other orthologs, we aligned Calreticulin sequences across four insect orders (Lepidoptera, Diptera, Coleoptera, and Hymenoptera). Whole sequence alignment of Calreticulin indicates that the C-terminal ends vary among species (Fig. S9A, Fig. S10A, Fig. S11A - Fig. S14A) and different orders have different C-terminal end patterns (Fig. S9B, Fig. S11B - Fig. S14B). Two conserved and unique motifs were found at the C-terminal end of Lepidopteran sequences (Fig. S9B, Fig. S10). Alignment results as FASTA Alignment output files can be found at https://zenodo.org/records/15477610.

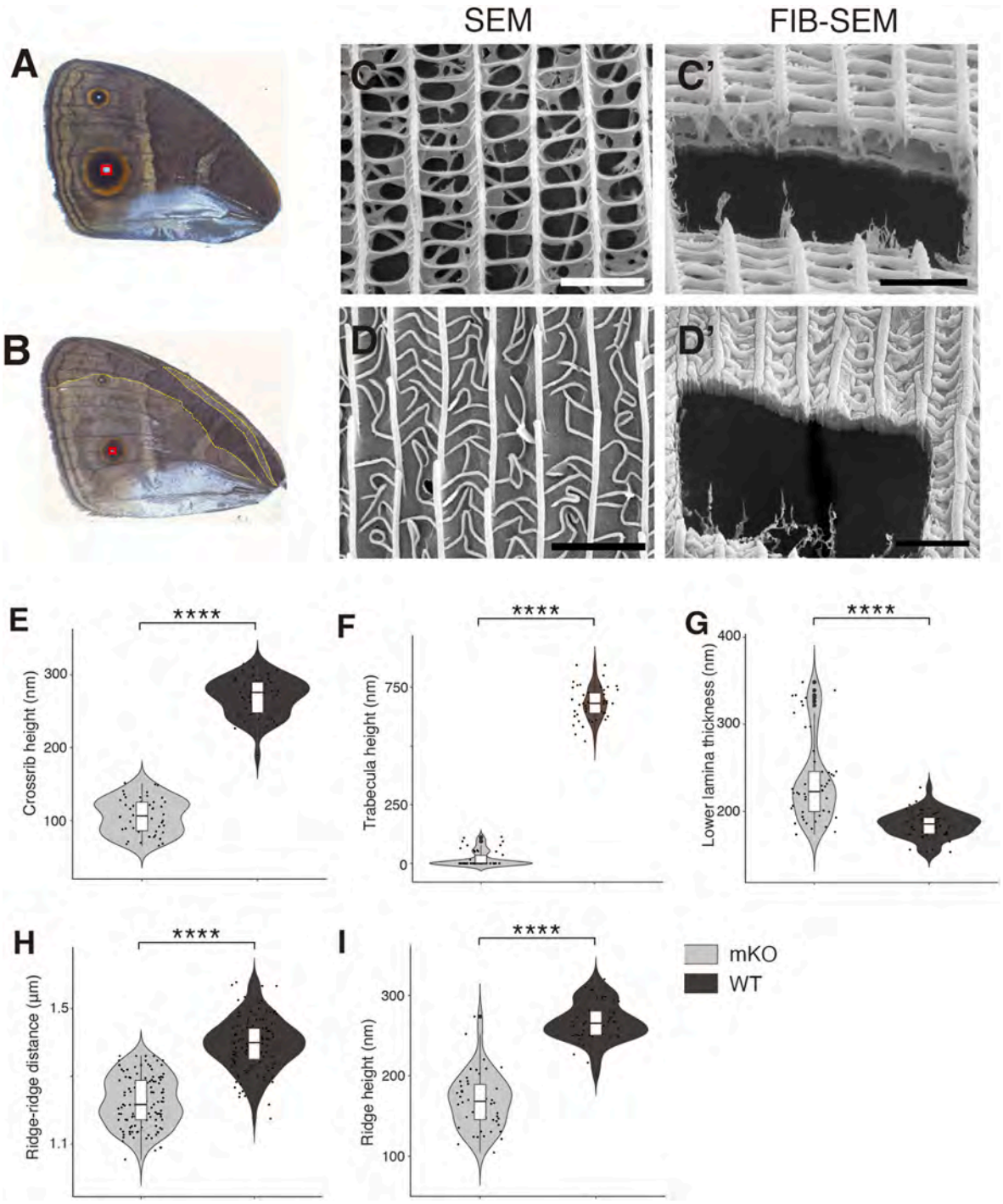

Fig. 6. WT eyespot-center white scale morphology was significantly distorted upon *calreticulin* knockout. SEM and FIB-SEM images of WT (C, C') and Cal-N M4 mKO white scales (D, D') were taken from the red-rectangle demarcated areas in A and B, respectively. Scale bars: 2 μm. (E–I) Violin plots of Cal-N M4 mKO and WT white scales crossrib and trabecula heights, lower lamina thickness, distance between adjacent ridges, and ridge height. Crossrib and trabecula heights, lower lamina thickness, and ridge height: n = 5, measurements = 50; adjacent ridge distance: n = 5, measurements = 125. ****: $p < 0.0001$. The central line in the violin plot indicates the median of the distribution, while the top and bottom of the box represent the third and first quartiles of the data, respectively. The whiskers show up to 1.5 times the interquartile range. (For interpretation of the references to color in this figure legend, the reader is referred to the Web version of this article.)

3. Discussion

In this study, we found evidence that the cuticular pillars (trabeculae) that transverse the lumen of dead scale cells, are likely formed by cuticle being deposited to the outside of finger-like invaginations of the plasma membrane in developing scale cells. Our STED and TEM data support the idea that these pillars are formed outside the scale cell, topologically, while clearly transversing it from one side to the other. We also discovered that the classic ER-resident protein Calreticulin cannot be used as an ER membrane marker at the stages of scale development examined here (77–88 % of pupal development), as the signal of the antibody targeting this protein was found embedded in the cuticle of *B. anynana* wing scales, both in the upper and lower laminae, and inside the trabeculae that transversed the scales (Fig. 1). Although

Table 2
Summary of *calreticulin* mutant phenotypes of different scale types.

scale type	Phenotype					
	color	ridges	crossribs	trabeculae	windows	Degree of morphological change
dorsal brown, ventral brown, ventral black	scales became paler	no obvious change	formed a beaded-bracelet shape between ridges; adjacent crossribs distance became shorter	became shorter or missing	most windows became closed with a thin cuticular film	Moderate - Changes in crossribs and trabeculae.
ventral orange	no change	no obvious change	formed a beaded-bracelet shape between ridges; adjacent crossribs distance became shorter	became shorter or missing	most windows became closed with a thin cuticular film	Moderate - Changes in crossribs and trabeculae.
ventral white	no change	adjacent ridges distance became shorter	became severely disordered	most were missing	window-like structure disappeared as crossribs pointed in all directions	Severe - most scales were missing. Changes in crossribs, missing trabeculae.
ventral silver	no change	no obvious change	no obvious change	no obvious change	no obvious change	Slight - no visible change

Western blot analysis indicates that the anti-*H. sapiens* Calreticulin antibody recognizes both Calreticulin and Calnexin in *B. anynana*, functional studies confirm that Calreticulin specifically plays a key role in wing scale cuticle formation.

Mutations targeting *calreticulin* significantly altered the morphology of all the scales with well-defined crossribs (brown, black, orange and white scales) (Fig. 4, Fig. 6C-D', Fig. S6G and H, Fig. S8A-C) and made brown and black scales (but not orange scales) lose pigmentation (Fig. S5, Fig. S6A-F'', Fig. S8D–G''). In general, mutations in *calreticulin* affected the formation of crossribs and their orientation, and inhibited the formation of trabeculae below the crossribs, making them shorter or missing (Fig. 4, Fig. S7). White scales were most severely affected by these mutations (Fig. 6). They had severely disordered crossribs (Fig. 6D) and an absent scale lumen (Fig. 6D') with no trabeculae (Fig. 6F). It is likely that white scales formed but were lost upon adult emergence, perhaps due to the large morphological alterations (Fig. 3B). In contrast, silver scales, which do not produce crossribs, were only slightly affected in their morphology, and their development does not seem to rely on Calreticulin (Fig. 5).

There are at least two possible explanations for why only brown or black scales showed lower levels of pigmentation, but not orange scales. Orange scales contain primarily ommochrome pigments (How et al., 2023; Banerjee et al., 2024), whereas brown scales contain melanins (Matsuoka and Monteiro, 2018). If ommochromes are preferentially deposited along longitudinal ridges, and melanins preferentially deposited in crossribs and trabeculae, as proposed for *B. anynana* (Banerjee et al., 2024), then, preventing these latter structures from forming would prevent melanins from being deposited in the mass of the scale, leading to lighter scales, but would not affect ommochrome deposition. An alternative explanation for the reduced pigmentation effects exclusively in brown/black scales is that Calreticulin mutations are known to lead to misfolding of an enzyme in the melanin pathway, tyrosinase, which would affect melanin production, but not ommochrome production (Petrescu et al., 1997; Liedy, 2005). Distinguishing between these two alternatives would require further study.

3.1. Trabecula formation during development

Here we propose a model of trabeculae formation based on our experimental observations. We noted that in *B. anynana* the lower lamina and ridges form first, followed by the crossribs and the pillar-like trabeculae, a pattern previously noted in other species (Ghiradella, 1989, Dinwiddie et al., 2014). When crossribs first formed they were thin, but later became thicker. In *calreticulin* mutants, the crossribs remain thin, and it is possible that the shorter or missing trabeculae in these mutants result from failed growth of trabeculae below these thin crossribs. In our model, we propose that at the late pupal developmental stage, with the involvement of Calreticulin, crossribs become thick. Meanwhile, at points along these crossribs, fingers of plasma membrane invaginate towards the interior lumen of the cell, fuse with the membrane on the other side of the scale and form an extracellular channel into which cuticle is deposited to form trabeculae (Fig. 7B and C). We name these points "trabecula starting points" (Fig. 7B). The scale cell then dies, leaving its cuticular skeleton behind where the cuticle transverses the scale (Fig. 7D). When *calreticulin* is mutated, crossrib formation is disrupted, impairing trabecula starting points located at crossribs, and preventing trabecula from forming (Fig. 7B' and C'). Upon cell death, and without the support of pillar-like trabeculae, the upper surface collapses and is found fused to the lower lamina (Fig. 7D').

In silver scales, there are complex trabeculae connecting the two laminae (Fig. 5C''), but they seem to originate at the lamina and not at the thin microribs. Given that *calreticulin* mutations do not affect silver-scale trabeculae morphology, we speculate that Calreticulin is dispensable for the formation of those web-like trabeculae.

3.2. The role of calreticulin in structural coloration

This work, as well as other recent studies, has started to unravel the genetic and developmental basis of structural color-producing mechanisms in butterflies. Structural colors in butterfly scales arise from the interaction of light with the cuticular properties (mass density and fine morphology) of the scales (Cuthill et al., 2017, Wilts and Vignolini, 2019, Lloyd and Nadeau, 2021, Balakrishnan et al., 2023b, Finet, 2024, Balakrishnan et al., 2025). Here we found that Calreticulin is an essential protein for the regulation of trabeculae height, as well as ridge height, two structures essential for the formation of vibrant structural colors in other butterflies. For instance, a recent study found that ridge height influences the hue, intensity, and saturation of ridge coloration (Finet et al., 2024). Similarly, the height of the trabeculae was found to play a crucial role in determining the thickness of the air-filled space between the upper and lower lamina, a key parameter for tuning the silver coloration observed in certain butterfly scales (Dolinko et al., 2021; Prakash et al., 2022). We propose that changes in the regulation of Calreticulin production may have played a role in changes in trabeculae height and ridge height across evolution, which may have had a direct impact on the production of structural colors.

3.3. Evolution of scales

Scales with fused upper and lower laminae are widely considered primitive (Kristensen, 1970; Zhang et al., 2018; Kilchoer et al., 2019). The evolutionary origins of wing scales can be traced back to primitive insect groups within Amphiesmenoptera, which includes Trichoptera (caddisflies) and the extinct Tarachoptera. Fossil and morphological evidence suggest that wing scales evolved from sensory bristles (setae) that gradually diversified into the complex structures observed in modern butterflies (Zhang et al., 2018; Monteiro et al., 2025). Scales found in fossilized Tarachoptera (*Kinitocelis brevicostata*) specimens and basal lepidopteran groups such as Micropterigidae (*Micropterix aureatella* and *Micropterix tunbergella*) consistently exhibit fused upper and

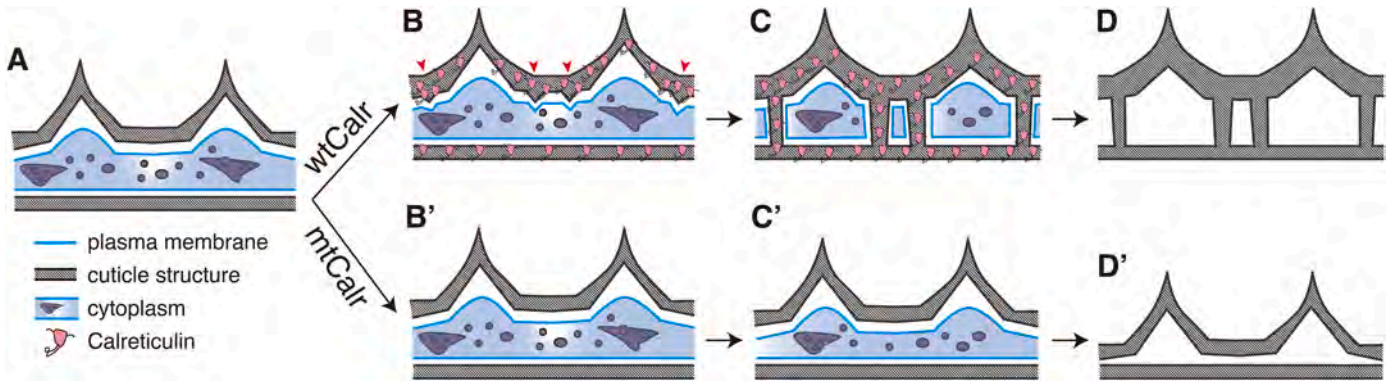

Fig. 7. Model for how Calreticulin affects the formation of crossribs and trabeculae. (A) At ~70 % development, ridges and thin crossribs have formed. (B–C) "Trabecula starting points" (red arrowheads) start to form from further-developed crossribs with the help of WT Calreticulin. (B'-C') Mutating Calreticulin impairs crossrib formation, which impairs trabecula formation. (D, D') Cells die after scale development is complete, leaving their cuticular skeleton behind. (D') Without trabecula support, cell death results in the upper surface structures (ridges and crossribs) becoming attached to the lower lamina. (For interpretation of the references to color in this figure legend, the reader is referred to the Web version of this article.)

lower laminae and lack trabeculae (Kristensen, 1970; Zhang et al., 2018; Kilchoer et al., 2019).

Interestingly, these primitive features are not exclusive to basal-branching or extinct species but can also be found in certain specialized wing scales of modern Lepidoptera. Examples include the glass scales in *Graphium sarpedon* butterflies (Stavenga et al., 2012) and the vertical scales in transparent patches in *Phanus vitreus* butterflies (Finet et al., 2023), which are specialized polarizing reflectors.

In contrast, most pigmented scales have undergone further specialization, developing elaborate ridges, cross-ribbing, and perforations. These modifications led to the formation of hollow structures supported by pillar-like trabeculae, enabling pigment storage and structural coloration through light refraction and diffraction. Among these adaptations, the emergence of pillar-like trabeculae represents a key evolutionary innovation in the transition toward more complex hollow-scale architectures. Based on these findings, we propose that *calreticulin* was co-opted by scale cells during evolution, facilitating the emergence of pillar-like trabeculae and consequently contributing to the formation of hollow-scale architectures.

3.4. *The lectin domain and the C-terminal end of calreticulin are potential functional elements in the scale nanostructure development*

Calreticulin is a pleiotropic protein that is found in all eukaryotic cells. The functions of Calreticulin include but are not limited to calcium buffering, chaperoning glycoproteins, cell adhesion, antigen presentation on the cell surface, initiation of apoptotic-cell removal, and wound healing (Coppolino et al., 1997; Ogden et al. 2001; Gardai et al., 2005; Obeid et al., 2007; Michalak et al., 2009; Fucikova et al., 2021; Sawaya et al., 2023). The pleiotropic nature of this protein explains why most injected individuals (96 %) in the Cal-N CRISPR died during growth, indicating Calreticulin's essential function for embryonic survival. However, *calreticulin* mutations did not influence wing cell survival as genotyping results confirmed that most wing cell clones affected were homozygous mutants with frameshifts (Fig. 3C, Table 1, Supplementary data- Cal Mutant genotype.xlsx).

To explain how Calreticulin might impact scale cuticle development, we explored its protein sequence in detail. There are three main domains in Calreticulin proteins: N-, P-, and C- domains (Fig. 3A, Fig. S3). N- and P- domains are important for the glycoprotein chaperone function and the C-domain is important for the calcium buffering function (Michalak et al., 2009; Wang et al., 2012; Fucikova et al., 2021). The N-terminus contains a carbohydrate-binding site in a globular lectin domain. Lectins, such as Conconvalina (ConA), WGA, and Soybean agglutinin (SBA), are a group of glycoproteins that can bind glycans or sugars (Ni and Tizard, 1996, Kremsreiter et al., 2021). Chitin, a polymer of N-acetyl-glucosamine, is a type of sugar (an amide derivative of glucose). Therefore, the lectin activity of Calreticulin makes it a potential chitin-binding protein, which would explain its presence in the cuticular matrix of developing scales (Fig. 1), and its newly discovered function in scale crossrib and trabecula development.

In this study, however, Cal-C CRISPR mutants showed similar phenotypes as Cal-N mutants, suggesting that another functional element may exist in the C-terminal end (Fig. S3). Calreticulin C-terminal ends vary dramatically across insect orders and lepidopterans exhibit two unique amino acid motifs (Fig. S9B, Fig. S11 - Fig. S14). We speculate that these unique motifs might also be involved in scale cuticle development, but future work is required to test this hypothesis. Furthermore, it is worth noting that scales from butterflies in families other than Nymphalidae do not have the typical "ridge-crossrib-trabecula-lower laminae" nanostructures. The interior lumen of these scales can have honeycomb lattices, perforated multilayer lattices, and multiple other cuticular structures (Ghiradella and Radigan, 1976; Ghiradella, 1984; Ghiradella, 1985; Prum et al., 2006; Seah and Saranathan, 2023). It might be interesting to explore how Calreticulin functions in the formation of all these nanostructures.

4. Materials and methods

4.1. *Butterfly husbandry*

B. anynana butterflies were reared at 27 °C as described in a previous publication (Prakash and Monteiro, 2018). To harvest pupal wings at specific developmental time points, the time of pupation was recorded.

4.2. *TEM immunogold labeling*

Butterfly pupal wings were fixed with 4 % formaldehyde in 0.1 M PB (0.1 M Phosphate Buffer, pH7.4) for 12–24 h at 4 °C, rinsed in 0.1 M PB for 3 × 10 min and quenched in 0.1 M Glycine in 0.1 M PB. The wings were then incubated in 0.2 M Sucrose in 0.1 M PB for 2 × 15min at room temperature. Dehydration was performed by incubating wings in two changes of 70 % ethanol 30 min each, then in LR white resin and 70 % ethanol (2:1) mixture for 1 h, and in three changes of pure LR white resin for 1 h each. Wings were incubated in the last change of LR white resin overnight at room temperature. Samples were then placed in the bottom of a gelatin capsule, filled with LR white resin to the brim, and polymerized in a 60 °C oven for 24–48 h or longer. Those EM blocks were trimmed and sectioned at 90–100 nm. Sections were rinsed for 2 × 2 min by placing grids on large droplets of TBS-Tween (0.05 M TBS, 0.05 %

Tween 20, pH 7.6) and blocked in IHC Ultra Serum Blocking buffer (1 % BSA, 3 % Normal Serum, 0.1 % Fish Gelatin, 0.05 % Sodium Azide in 0.05 M TBS, pH 7.6) for 30 min. For primary antibody labeling, sections were incubated on droplets of rabbit anti-Calreticulin antibody (ab2907, Abcam) diluted 20 times in Universal Antibody Diluent (ab79995, Abcam), overnight at 4 °C. This was followed by rinsing on large droplets of TBS-Tween for 6 × 2 min. For the negative control, the same volume of Universal Antibody Diluent without primary antibody was used. For secondary antibody staining, the sections were incubated on droplets of secondary immunogold-conjugated antibodies (Anti-Rabbit IgG (whole molecule) – This antibody was produced in a goat, and conjugated with 5 nm gold nanoparticles (colloidal gold, G7277, Sigma-Aldrich) at 1:40 in 1 % serum/TBST + 0.5 % polyethylene glycol for 1 h at room temperature. Sections were post-fixed on droplets of 2.5 % glutaraldehyde in 0.1 M PB for 10 min and stained with lead citrate for 5 min. Images were acquired on a JEOL 1400Flash TEM (JEOL Ltd. Japan).

4.3. Immunofluorescence

To visualize Armadillo proteins in wing scale cross sections, the EM resin blocks generated for immunogold staining were sectioned at 200–300 nm and attached onto glass slides. These sections were rinsed for 2 × 2 min with TBS-Tween and blocked in IHC Ultra Serum Blocking buffer for 2 h. For primary antibody labeling, sections were incubated in 1:40 diluted house-made Rat anti-*Bicyclus* Armadillo antibody (Banerjee et al., 2023) in Universal Antibody Diluent (ab79995, abcam) overnight at 4 °C. This was followed by rinsing on TBS-Tween for 6 × 2 min. For the negative control, the same volume of Universal Antibody Diluent without primary antibody was used. For secondary antibody staining, 1:50 diluted Goat Anti-Rat IgG H&L (Alexa Fluor® 647) (ab150159, abcam) was applied on the sections for 2 h. After washing with TBS-Tween for another 6 × 2 min, the sections were stained with wheat germ agglutinin (WGA) conjugated with Alexa Fluor™555 (w32464, ThermoFisher) and mounted in Abberior mounting medium. The slides were examined with a Zeiss LSM900 confocal microscope and an Abberior STED microscope (STEDYCON, Abberior) to acquire images.

4.4. CRISPR/Cas9 deletion

The CRISPR knockout method through embryonic injection was described previously (Banerjee and Monteiro, 2018). Instead of single guide RNAs (sgRNA), in this study, CRISPR using crRNA-tracrRNA duplex was carried out following the protocol provided by IDT (Integrated DNA Technologies, U.S.A). Cal-N and Cal-C crRNAs were designed, and their on-target score was assessed by the Custom Alt-R™ CRISPR-Cas9 guide RNA design service, IDT. Both crRNA and tracrRNA were synthesized by IDT. 4 μl Nuclease-Free Duplex Buffer (IDT) was mixed with 0.5 μl 100 μM crRNA and 0.5 μl 100 μM tracrRNA. The mixture was heated at 95 °C for 5 min and cooled down to room temperature. 0.5 μl of 10 μg/μL Cas9 protein solution (Alt-R™ S.p. Cas9 Nuclease V3, 1081058, IDT) was diluted in 5 μl Cas9 working concentration buffer (20 mM HEPES; 150 mM KCl, pH 7.5) and mixed with 0.05 μmol crRNA-tracRNA duplex, followed by incubating at 37 °C for 5 min to form RNP. The Cas9 RNP complex was then ready for injection. All crRNA and primers used for NGS genotyping were summarized in Table S1.

4.5. Optical imaging and UV–VIS–NIR microspectrophotometry

Light microscope images of individual scales were recorded using the 20X objective lens of a uSight-2000-Ni microspectrophotometer (Technospex Pte. Ltd., Singapore) and a Touptek U3CMOS-05 camera. Scales from either WT or mKO areas were taken, mounted on a glass slide, and viewed using Llumins Toupview microscope camera software. For silver scales, the light source was provided by a Thorlabs Mercury-Xenon Short-Arc Light Source (SLS402, ThorLabs Inc., New Jersey, USA). To obtain better images, only intact scales were chosen and images were taken at different focal distances. Z-stacking was carried out using EDF function (Process > EDF …) in Toupview. Maximum Contrast with default settings, followed by no Auto Align, was used as the EDF method.

To measure absorbance, scales were mounted in clove oil (C8392, Sigma-Aldrich, refractive index = 1.532), with a similar refractive index to chitin. Matching the reflective indexes minimizes the production of structural colors and allows the quantification of pigmentary-based colors alone. The absorbance spectrum was measured for individual scales using a 20X objective, with 100 ms integration time and 10x averaging. For each scale type, average values were taken from three measurements of each scale, and six to eight individual scales were measured. Spectra with useable range between 400 and 700 nm were shown. Analyses and spectral plots were done in R Studio 2023.03.0 Build 386 with R version 4.2.3 (2023-03-15) (R Core Team, 2013) URL: https://www.R-project.org/.) using the R-package pavo (v 2.7) (Maia et al., 2019).

To measure reflectance, an aluminum reflector sheet was used as a reference for 100 % reflectance. Individual silver scales from a WT male forewing or the Cal-N M4 forewing were picked and mounted on glass slides and illuminated with the same light source as in the optical imaging of silver scales. Normal-incidence UV–VIS–NIR reflectance spectra with a useable range between 335 and 700 nm were collected using a high NA 100x objective. For each scale, three measurements were taken from three different areas of the scale surface, and five to ten scales were measured for each scale type.

Statistical analysis of the absorbance and reflectance spectra changes at 400 nm, 500 nm, 600 nm, and 700 nm wavelength were performed as described in a previous publication (Thayer et al., 2020). The results are shown in Table S2 xlsx.

4.6. Focused ion beam scanning electron microscopy (FIB-SEM)

FIB-SEM method was described in previous publications (Prakash et al., 2022; Banerjee et al., 2024). Five to ten scales picked from each selected area of the wings were used for each sample. Images were taken with a FEI Versa 3D with the following settings: beam voltage 8 kV, beam current 12 pA at a 52° tilt. Image acquisition was performed in the same equipment with the following settings: beam voltage 5 kV, beam current 13 pA.

4.7. Scanning electron microscopy (SEM)

More than 10 scales from each selected area of the wings were picked using insect pins and individually mounted onto carbon tape stuck on a SEM stub. The scales were then sputter-coated with platinum using a JFC-1600 auto Fine Coater (JEOL Ltd. Japan). Images were obtained using a JEOL JSM-6701F Field Emission Scanning Electron Microscope (FESEM) (JEOL Ltd. Japan).

4.8. Cross-sectional TEM

Pupal forewings at 131-h APF were dissected and fixed in 2.5 % Glutaraldehyde at 4 °C overnight, followed by three washes in PBS (20 min for one wash). Regular cross-sectional TEM was performed on stained samples using potassium ferrocyanide in osmium tetroxide for the post-fixation (1.5 % Potassium ferrocyanide $K_4[Fe(CN)_6]$ in 1 % Osmium Tetroxide) as described in a previous publication (Balakrishnan et al., 2023b). Images were acquired on a JEOL 1400Flash TEM (JEOL Ltd. Japan).

4.9. Measurements and statistical analysis

Measurements of thicknesses and distances were measured from SEM images using the Line tool implemented in Fiji (Schindelin et al., 2012).

For all parameters, repeated measurements were taken per scale with five scales sampled from one area. Due to the multilevel context of the datasets, we ran linear mixed-effects (LME) models using the R package nlme (Pinheiro et al., 2023) that allows coefficients to vary with respect to one or more grouping variables. Scale type, for example, dorsal brown cover or ventral brown ground, was treated as a fixed factor, and scale nested within individual butterfly as a random factor. The lack of homogeneity of variances among scale types prompted us to use the varIdent() function in the nlme package. Akaike information criterion (AIC) was used to compare different possible models and determine which one is the best fit for the data. Outcomes of the LME tests and the p-values are given in Supplementary data -Table S3.xlsx and Table S4.xlsx. Measurements were plotted using the R package ggplot 2 (Gómez-Rubio, 2017). For crossrib height, trabecula height, lower lamina thickness and ridge height, for each scale type, 5 individual scales were selected, and 10 individual measurements were taken within a scale. Total measurements = 50. For crossrib distance and ridge distance, for each scale type, 5 individual scales were selected, and 25 individual measurements were taken within a scale. Total measurements = 125.

4.10. Top-down transmission electron microscopy (TEM)

Formvar-coated TEM grids were glow-discharged for 30 s, at 5 mA using a Leica EM ACE200. Ten or more individual scales of the same color were picked from each selected wing area and placed on the discharged grids. Top-down TEM images were then taken using a JEOL 1400Flash TEM (JEOL Ltd. Japan).

4.11. Genotyping adult wings

Genotyping of crispants was carried out using a method described in a previous publication (Tian et al., 2024). After collecting a sufficient number of wing scales for characterization, such as absorbance/reflectance measurements and electron microscopy (EM) imaging, and only after these analyses were completed, genomic DNA was extracted from mutant adult wing patches showing both WT and mKO phenotypes (see an example in Fig. 3B) except Cal-N M4S, which was extracted from a pure mKO area of a Cal-N M4 forewing covered by silver scales. Next-generation sequencing (NGS) was performed on an Illumina iSeq 100 system, using 2x150bp paired-end (PE) sequencing. Sequence analyses were done using the online web-tool "CRISPR RGEN Tools" (http://www.rgenome.net/). Genotyping results are shown in (Fig. 3C, Table 1, Supplementary data- Cal Mutant genotype.xlsx).

4.12. Multiple alignments of insect calreticulin

The alignment was carried out using COBALT (Constraint-based Multiple Alignment Tool, https://www.ncbi.nlm.nih.gov/tools/cobalt/cobalt.cgi) by uploading the accession ID of Calreticulin proteins. We included 15 representative lepidopteran sequences from Nymphalidae, Papilionidae, Pieridae, Lycaenidae, Pyralidae, Noctuidae, Geometridae, Sphingidae, and Bombycidae; Eight representative dipteran sequences from Culicidae, Tephritidae, Cecidomyiidae, and Drosophilidae; Ten representative coleopteran sequences from Brentidae, Buprestidae, Chrysomelidae, Coccinellidae, Curculionidae, Lampyridae, Nitidulidae, Scarabaeidae, and Tenebrionidae; And eight representative hymenopteran sequences from Ampulicidae, Apoidea, Formicidae, Braconidae, Athaliidae, and Diprionidae. For the alignment of all four orders, all 41 representative Calreticulin sequences were uploaded. The accession ID and species information can be found in Supplementary data- Calreticulin_ACCESSION.xlsx.

4.13. Western blot

Western blotting was performed following (Choi et al., 2002; Tong et al., 2012). In short, hemolymph collected from 20 fifth-instar larvae was centrifuged at 3000×*g* at 4 °C for 10 min. He precipitated hemocytes were washed with 500 μl of anti-coagulation buffer (30 mM trisodium citrate, 26 mM citric acid, 20 mM EDTA, and 15 mM sodium chloride, 1 x protease inhibitor cocktail (Thermo Scientific™ 87785), pH 5.5) and resuspended with 100 μl of anti-coagulation buffer, followed by sonicated for 60 s at 4 °C and centrifuged at 22,000×*g* at 4 °C for 10 min. The supernatant was mixed with 5 μl SDS-PAGE loading buffer and separated on a 4–12 % NuPAGE Bis-Tris gel (Thermo Scientific™ NP032C) and transferred to a PVDF membrane (Millipore Corporation cat #K9PN0097). After blocking, the membrane was incubated with the 1: 2000 anti-Calreticulin (CRT) antibody (ab2907, Abcam), washed 3 × 5 min with TBST buffer, then incubated with 1:10000 goat anti-rabbit IgG H&L (HRP) (ab6721, Abcam), washed 3 times with TBST buffer, followed by incubation with Clarity Western ECL Substrate, (#1705061, Bio-Rad). Signals were detected with a Bio-Rad ChemiDoc Imaging System.

CRediT authorship contribution statement

Ru Hong: Writing – review & editing, Writing – original draft, Visualization, Validation, Project administration, Methodology, Investigation, Formal analysis, Data curation, Conceptualization. **Cédric Finet:** Writing – review & editing, Validation, Software, Formal analysis, Data curation. **Antónia Monteiro:** Writing – review & editing, Validation, Supervision, Project administration, Funding acquisition, Conceptualization.

Competing interest Statement

The authors declare no competing interests.

Acknowledgements

We thank Sim Aik Yong from the Electron Microscopy Unit (EMU) of Yong Loo Lin School of Medicine, NUS, for help with the EM section preparation, post-staining, and TEM operation, Cheng Liyan Sherona from the Department of Chemistry, NUS, for access and help with SEM, the Electron Microscopy Facility (EMF, NUS) for use of FIB-SEM, Abberior GmbH company for use of their super-resolution STEDYCON microscope, E. Chae' lab and Y. Yun for help with the genotyping NGS, Xin-Fu Yan from School of Biological Sciences, Nanyang Technological University, for help with the Western blotting, Deepan Balakrishnan for providing a top-down TEM protocol, and Tirtha Das Banerjee for providing the *B. anynana* Armadillo antibody. This research was supported by the National Research Foundation (NRF) Singapore under the Competitive Research Program (award NRF-CRP20-2017-0001) and the Ministry of Education, Singapore (award MOE-T2EP30222-0017).

Appendix A. Supplementary data

Supplementary data to this article can be found online at https://doi.org/10.1016/j.ydbio.2025.06.013.

Data availability

Data will be made available on request.

References

Balakrishnan, D., Prakash, A., Daurer, B., Kiat, J.O.J., Tan, Y.Z., Monteiro, A., Loh, N.D., 2023a. Potential large-area imaging of butterfly wing scales with transmission electron microscopy. Microsc. Microanal. 29 (Suppl. ment_1), 1207–1208.

Balakrishnan, D., Prakash, A., Daurer, B.J., Finet, C., Lim, Y.C., Monteiro, A., Loh, N.D., 2025. Correlative imaging provides novel insights into butterfly wing scales' coloration, structure, and density. 13th Asia Pacific Microscopy Congress 2025 (APMC13). ScienceOpen.

Balakrishnan, D., Prakash, A., Daurer, B.J., Finet, C., Lim, Y.C., Shen, Z., Thibault, P., Monteiro, A., Loh, N.D., 2023b. Nanoscale cuticle density variations correlate with pigmentation and color in butterfly wing scales. arXiv preprint arXiv:2305.16628.
Banerjee, T.D., Finet, C., Seah, K.S., Monteiro, A., 2024. Optix regulates nanomorphology of butterfly scales primarily via its effects on pigmentation. Front. Ecol. Evol. 12.
Banerjee, T.D., Monteiro, A., 2018. CRISPR-Cas9 mediated genome editing in Bicyclus anynana butterflies. Methods Protoc. 1 (2).
Banerjee, T.D., Monteiro, A., 2020. Molecular mechanisms underlying simplification of venation patterns in holometabolous insects. Development 147 (23).
Banerjee, T.D., Murugesan, S.N., Connahs, H., Monteiro, A., 2023. Spatial and temporal regulation of Wnt signaling pathway members in the development of butterfly wing patterns. Sci. Adv. 9 (30), eadg3877.
Binnington, K., Retnakaran, A., 1991. Physiology of the Insect Epidermis. CSIRO, Australia. East Melbourne, Vic.
Choi, J.Y., Whitten, M.M., Cho, M.Y., Lee, K.Y., Kim, M.S., Ratcliffe, N.A., Lee, B.L., 2002. Calreticulin enriched as an early-stage encapsulation protein in wax moth Galleria mellonella larvae. Dev. Comp. Immunol. 26 (4), 335–343.
Coppolino, M.G., Woodside, M.J., Demaurex, N., Grinstein, S., St-Arnaud, R., Dedhar, S., 1997. Calreticulin is essential for integrin-mediated calcium signalling and cell adhesion. Nature 386 (6627), 843–847.
Cox, R.T., Kirkpatrick, C., Peifer, M., 1996. Armadillo is required for adherens junction assembly, cell polarity, and morphogenesis during Drosophila embryogenesis. J. Cell Biol. 134 (1), 133–148.
Cuthill, I.C., Allen, W.L., Arbuckle, K., Caspers, B., Chaplin, G., Hauber, M.E., Hill, G.E., Jablonski, N.G., Jiggins, C.D., Kelber, A., 2017. The biology of color. Science 357 (6350), eaan0221.
Day, C.R., Hanly, J.J., Ren, A., Martin, A., 2019. Sub-micrometer insights into the cytoskeletal dynamics and ultrastructural diversity of butterfly wing scales. Dev. Dyn. 248 (8), 657–670.
De Giorgio, E., Giannios, P., Espinas, M.L., Llimargas, M., 2023. A dynamic interplay between chitin synthase and the proteins Expansion/Rebuf reveals that chitin polymerisation and translocation are uncoupled in Drosophila. PLoS Biol. 21 (1), e3001978.
de la Roche, M., Hamilton, C., Mortensen, R., Jeyaprakash, A.A., Ghosh, S., Anand, P.K., 2018. Trafficking of cholesterol to the ER is required for NLRP3 inflammasome activation. J. Cell Biol. 217 (10), 3560–3576.
Dinwiddie, A., Null, R., Pizzano, M., Chuong, L., Leigh Krup, A., Ee Tan, H., Patel, N.H., 2014. Dynamics of F-actin prefigure the structure of butterfly wing scales. Dev. Biol. 392 (2), 404–418.
Dolinko, A., Borgmann, L., Lutz, C., Curticean, E.R., Wacker, I., Vidal, M.S., Szischik, C., Donie, Y., Inchaussandague, M., Skigin, D., 2021. Analysis of the optical properties of the silvery spots on the wings of the Gulf Fritillary, Dione vanillae. Sci. Rep. 11 (1), 19341.
Finet, C., 2024. Developmental genetics of cuticular micro-and nano-structures in insects. Curr. Opin. Insect Sci., 101254
Finet, C., Bei, Y.Y., Saranathan, V., Ruan, Q., Monteiro, A., 2024. Ridge and crossrib height of butterfly wing scales is a toolbox for structural color diversity. bioRxiv, 2024.2003.2028.585318.
Finet, C., Ruan, Q., Bei, Y.Y., You En Chan, J., Saranathan, V., Yang, J.K., Monteiro, A., 2023. Multi-scale dissection of wing transparency in the clearwing butterfly Phanus vitreus. J. R. Soc. Interface 20 (202), 20230135.
Forman, K.A., Thulin, C.D., 2022. Ommochrome wing pigments in the monarch butterfly Danaus plexippus (Lepidoptera: Nymphalidae). J. Insect Sci. 22 (6).
Fucikova, J., Spisek, R., Kroemer, G., Galluzzi, L., 2021. Calreticulin and cancer. Cell Res. 31 (1), 5–16.
Gardai, S.J., McPhillips, K.A., Frasch, S.C., Janssen, W.J., Starefeldt, A., Murphy-Ullrich, J.E., Bratton, D.L., Oldenborg, P.A., Michalak, M., Henson, P.M., 2005. Cell-surface calreticulin initiates clearance of viable or apoptotic cells through trans-activation of LRP on the phagocyte. Cell 123 (2), 321–334.
Ghiradella, H., 1974. Development of ultraviolet-reflecting butterfly scales: how to make an interference filter. J. Morphol. 142 (4), 395–409.
Ghiradella, H., 1984. Structure of iridescent Lepidopteran scales: variations on several Themes 1. Ann. Entomol. Soc. Am. 77 (6), 637–645.
Ghiradella, H., 1985. Structure and development of iridescent Lepidopteran scales: the Papilionidae as a showcase family. Ann. Entomol. Soc. Am. 78 (2), 252–264.
Ghiradella, H., 1989. Structure and development of iridescent butterfly scales: lattices and laminae. J. Morphol. 202 (1), 69–88.
Ghiradella, H., 1991. Light and color on the wing: structural colors in butterflies and moths. Appl. Opt. 30 (24), 3492–3500.
Ghiradella, H., 1994. Structure of butterfly scales: patterning in an insect cuticle. Microsc. Res. Tech. 27 (5), 429–438.
Ghiradella, H., Radigan, W., 1976. Development of butterfly scales. II. Struts, lattices and surface tension. J. Morphol. 150 (2), 279–297.
Giraldo, M.A., Stavenga, D.G., 2008. Wing coloration and pigment gradients in scales of pierid butterflies. Arthropod Struct. Dev. 37 (2), 118–128.
Gómez-Rubio, V., 2017. ggplot 2-elegant graphics for data analysis. J. Stat. Software 77, 1–3.
Hell, S.W., Wichmann, J., 1994. Breaking the diffraction resolution limit by stimulated emission: stimulated-emission-depletion fluorescence microscopy. Opt. Lett. 19 (11), 780–782.
Hirata, K., Otaki, J.M., 2019. Real-time in vivo imaging of the developing pupal wing tissues in the pale grass blue butterfly zizeeria maha: establishing the lycaenid system for multiscale bioimaging. J Imag. 5 (4).
How, S.H.C., Banerjee, T.D., Monteiro, A., 2023. Vermilion and cinnabar are involved in ommochrome pigment biosynthesis in eyes but not wings of Bicyclus anynana butterflies. Sci. Rep. 13 (1), 9368.
Iwata, M., Ohno, Y., Otaki, J.M., 2014. Real-time in vivo imaging of butterfly wing development: revealing the cellular dynamics of the pupal wing tissue. PLoS One 9 (2), e89500.
Kilchoer, C., Steiner, U., Wilts, B.D., 2019. Thin-film structural coloration from simple fused scales in moths. J. R. Soc. Interface Focus 9 (1), 20180044.
Klampfl, T., Gisslinger, H., Harutyunyan, A.S., Nivarthi, H., Rumi, E., Milosevic, J.D., Them, N.C., Berg, T., Gisslinger, B., Pietra, D., Chen, D., Vladimer, G.I., Bagienski, K., Milanesi, C., Casetti, I.C., Sant'Antonio, E., Ferretti, V., Elena, C., Schischlik, F., Cleary, C., Six, M., Schalling, M., Schonegger, A., Bock, C., Malcovati, L., Pascutto, C., Superti-Furga, G., Cazzola, M., Kralovics, R., 2013. Somatic mutations of calreticulin in myeloproliferative neoplasms. N. Engl. J. Med. 369 (25), 2379–2390.
Klowden, M.J., 2013. Physiological Systems in Insects. Academic press.
Kremsreiter, S.M., Kroell, A.H., Weinberger, K., Boehm, H., 2021. Glycan-lectin interactions in cancer and viral infections and how to disrupt them. Int. J. Mol. Sci. 22 (19).
Kristensen, N., 1970. Morphological observations on the wing scales in some primitive Lepidoptera (Insecta). J. Ultra. Res. 30 (3–4), 402–410.
Liedy, W., 2005. Do calnexin and calreticulin have a role in melanin formation? IUBMB Life 57 (6), 455–457.
Liu, X., Cooper, A.M.W., Zhang, J., Zhu, K.Y., 2019. Biosynthesis, modifications and degradation of chitin in the formation and turnover of peritrophic matrix in insects. J. Insect Physiol. 114, 109–115.
Lloyd, V.J., Burg, S.L., Harizanova, J., Garcia, E., Hill, O., Enciso-Romero, J., Cooper, R. L., Flenner, S., Longo, E., Greving, I., Nadeau, N.J., Parnell, A.J., 2024. The actin cytoskeleton plays multiple roles in structural colour formation in butterfly wing scales. Nat. Commun. 15 (1), 4073.
Lloyd, V.J., Nadeau, N.J., 2021. The evolution of structural colour in butterflies. Curr. Opin. Genet. Dev. 69, 28–34.
Maia, R., Gruson, H., Endler, J.A., White, T.E., 2019. "pavo 2: new tools for the spectral and spatial analysis of colour in R.". Methods Ecol. Evol. 10 (7), 1097–1107.
Matsuoka, Y., Monteiro, A., 2018. Melanin pathway genes regulate color and morphology of butterfly wing scales. Cell Rep. 24 (1), 56–65.
McDougal, A.D., Kang, S., Yaqoob, Z., So, P.T.C., Kolle, M., 2021. In vivo visualization of butterfly scale cell morphogenesis in Vanessa cardui. Proc. Natl. Acad. Sci. U. S. A. 118 (49).
Merzendorfer, H., 2006. Insect chitin synthases: a review. J. Comp. Physiol. B 176 (1), 1–15.
Merzendorfer, H., Zimoch, L., 2003. Chitin metabolism in insects: structure, function and regulation of chitin synthases and chitinases. J. Exp. Biol. 206 (Pt 24), 4393–4412.
Michalak, M., Groenendyk, J., Szabo, E., Gold, L.I., Opas, M., 2009. Calreticulin, a multi-process calcium-buffering chaperone of the endoplasmic reticulum. Biochem. J. 417 (3), 651–666.
Monteiro, A., Murugesan, S.N., Prakash, A., Papa, R., 2025. The developmental origin of novel complex morphological traits in lepidoptera. Ann. Rev. Entomol. 70 (1), 421–439.
Moretti, J., Roy, S., Bozec, D., Martinez, J., Chapman, J.R., Ueberheide, B., Lamming, D. W., Chen, Z.J., Horng, T., Yeretssian, G., Green, D.R., Blander, J.M., 2017. STING senses microbial viability to orchestrate stress-mediated autophagy of the endoplasmic reticulum. Cell 171 (4), 809–823 e813.
Nakazato, Y., Otaki, J.M., 2023a. Live detection of intracellular chitin in butterfly wing epithelial cells in vivo using fluorescent brightener 28: implications for the development of scales and color patterns. Insects 14 (9).
Nakazato, Y., Otaki, J.M., 2023b. Protein delivery to insect epithelial cells in vivo: potential application to functional molecular analysis of proteins in butterfly wing development. BioTech (Basel) 12 (2).
Nangalia, J., Massie, C.E., Baxter, E.J., Nice, F.L., Gundem, G., Wedge, D.C., Avezov, E., Li, J., Kollmann, K., Kent, D.G., Aziz, A., Godfrey, A.L., Hinton, J., Martincorena, I., Van Loo, P., Jones, A.V., Guglielmelli, P., Tarpey, P., Harding, H.P., Fitzpatrick, J.D., Goudie, C.T., Ortmann, C.A., Loughran, S.J., Raine, K., Jones, D.R., Butler, A.P., Teague, J.W., O'Meara, S., McLaren, S., Bianchi, M., Silber, Y., Dimitropoulou, D., Bloxham, D., Mudie, L., Maddison, M., Robinson, B., Keohane, C., Maclean, C., Hill, K., Orchard, K., Tauro, S., Du, M.Q., Greaves, M., Bowen, D., Huntly, B.J.P., Harrison, C.N., Cross, N.C.P., Ron, D., Vannucchi, A.M., Papaemmanuil, E., Campbell, P.J., Green, A.R., 2013. Somatic CALR mutations in myeloproliferative neoplasms with nonmutated JAK2. N. Engl. J. Med. 369 (25), 2391–2405.
Ni, Y., Tizard, I., 1996. Lectin-carbohydrate interaction in the immune system. Vet. Immunol. Immunopathol. 55 (1–3), 205–223.
Nishida, K., Adachi, H., Moriyama, M., Futahashi, R., Hanson, P.E., Kondo, S., 2023. Butterfly wing color made of pigmented liquid. Cell Rep. 42 (8), 112917.
Nowell, R.W., Elsworth, B., Oostra, V., Zwaan, B.J., Wheat, C.W., Saastamoinen, M., Saccheri, I.J., Van't Hof, A.E., Wasik, B.R., Connahs, H., 2017. A high-coverage draft genome of the mycalesine butterfly Bicyclus anynana. GigaScience 6 (7), gix035.
Obeid, M., Tesniere, A., Ghiringhelli, F., Fimia, G.M., Apetoh, L., Perfettini, J.L., Castedo, M., Mignot, G., Panaretakis, T., Casares, N., Metivier, D., Larochette, N., van Endert, P., Ciccosanti, F., Piacentini, M., Zitvogel, L., Kroemer, G., 2007. Calreticulin exposure dictates the immunogenicity of cancer cell death. Nat. Med. 13 (1), 54–61.
Ogden, C.A., deCathelineau, A., Hoffmann, P.R., Bratton, D., Ghebrehiwet, B., Fadok, V. A., Henson, P.M., 2001. C1q and mannose binding lectin engagement of cell surface calreticulin and CD91 initiates macropinocytosis and uptake of apoptotic cells. J. Exp. Med. 194 (6), 781–795.
Peifer, M., Sweeton, D., Casey, M., Wieschaus, E., 1994. Wingless signal and Zeste-white 3 kinase trigger opposing changes in the intracellular distribution of Armadillo. Development 120 (2), 369–380.

Petrescu, S.M., Petrescu, A.J., Titu, H.N., Dwek, R.A., Platt, F.M., 1997. Inhibition of N-glycan processing in B16 melanoma cells results in inactivation of tyrosinase but does not prevent its transport to the melanosome. J. Biol. Chem. 272 (25), 15796–15803.
Pietra, D., Rumi, E., Ferretti, V.V., Di Buduo, C.A., Milanesi, C., Cavalloni, C., Sant'Antonio, E., Abbonante, V., Moccia, F., Casetti, I.C., Bellini, M., Renna, M.C., Roncoroni, E., Fugazza, E., Astori, C., Boveri, E., Rosti, V., Barosi, G., Balduini, A., Cazzola, M., 2016. Differential clinical effects of different mutation subtypes in CALR-mutant myeloproliferative neoplasms. Leukemia 30 (2), 431–438.
Pinheiro, J., Bates, D., R. C. Team, 2023. nlme: linear and nonlinear mixed effects models. R Package Version 3.1-162, vol. 3. Team tRDC, pp. 1–86.
Prakash, A., Finet, C., Banerjee, T.D., Saranathan, V., Monteiro, A., 2022. Antennapedia and optix regulate metallic silver wing scale development and cell shape in Bicyclus anynana butterflies. Cell Rep. 40 (1), 111052.
Prakash, A., Monteiro, A., 2018. Apterous A specifies dorsal wing patterns and sexual traits in butterflies. Proc. Biol. Sci. 285 (1873).
Prum, R.O., Quinn, T., Torres, R.H., 2006. Anatomically diverse butterfly scales all produce structural colours by coherent scattering. J. Exp. Biol. 209 (Pt 4), 748–765.
R Core Team, R., 2013. R: A Language and Environment for Statistical Computing. R foundation for statistical computing Vienna, Austria.
Saccheri, I., null, n., null, n., null, n., null, n., 2023. The genome sequence of the Squinting Bush Brown, Bicyclus anynana (Butler, 1879) [version 1; peer review: 2 approved]. Wellcome Open Res. 8 (280).
Sawaya, A.P., Vecin, N.M., Burgess, J.L., Ojeh, N., DiBartolomeo, G., Stone, R.C., Pastar, I., Tomic-Canic, M., 2023. Calreticulin: a multifunctional protein with potential therapeutic applications for chronic wounds. Front. Med. 10, 1207538.
Schindelin, J., Arganda-Carreras, I., Frise, E., Kaynig, V., Longair, M., Pietzsch, T., Preibisch, S., Rueden, C., Saalfeld, S., Schmid, B., Tinevez, J.-Y., White, D.J., Hartenstein, V., Eliceiri, K., Tomancak, P., Cardona, A., 2012. Fiji: an open-source platform for biological-image analysis. Nat. Methods 9 (7), 676–682.
Schrag, J.D., Bergeron, J.J.M., Li, Y., Borisova, S., Hahn, M., Thomas, D.Y., Cygler, M., 2001. The structure of calnexin, an ER chaperone involved in quality control of protein folding. Mol. Cell 8 (3), 633–644.
Seah, K.S., Saranathan, V., 2023. Hierarchical morphogenesis of swallowtail butterfly wing scale nanostructures. eLife 12.
Sobala, L.F., Wang, Y., Adler, P.N., 2015. ChtVis-Tomato, a genetic reporter for in vivo visualization of chitin deposition in Drosophila. Development 142 (22), 3974–3981.
Stavenga, D.G., Matsushita, A., Arikawa, K., Leertouwer, H.L., Wilts, B.D., 2012. Glass scales on the wing of the swordtail butterfly Graphium sarpedon act as thin film polarizing reflectors. J. Exp. Biol. 215 (4), 657–662.
Thayer, R.C., Allen, F.I., Patel, N.H., 2020. Structural color in Junonia butterflies evolves by tuning scale lamina thickness. eLife 9, e52187.
Tian, S., Asano, Y., Das Banerjee, T., Komata, S., Wee, J.L.Q., Lamb, A., Wang, Y., Murugesan, S.N., Fujiwara, H., Ui-Tei, K., Wittkopp, P.J., Monteiro, A., 2024. A microRNA is the effector gene of a classic evolutionary hotspot locus. Science 386 (6726), 1135–1141.
Tong, X., Lindemann, A., Monteiro, A., 2012. Differential involvement of Hedgehog signaling in butterfly wing and eyespot development. PLoS One 7 (12), e51087.
Vukusic, P., Sambles, J.R., 2003. Photonic structures in biology. Nature 424 (6950), 852–855.
Wan, H., Wang, Q., Chen, X., Zeng, Q., Shao, Y., Fang, H., Liao, X., Li, H.S., Liu, M.G., Xu, T.L., Diao, M., Li, D., Meng, B., Tang, B., Zhang, Z., Liao, L., 2020. WDR45 contributes to neurodegeneration through regulation of ER homeostasis and neuronal death. Autophagy 16 (3), 531–547.
Wang, H., Christenson, L.K., Kinsey, W.H., 2022. Changes in cortical endoplasmic reticulum clusters in the fertilized mouse oocytedagger. Biol. Reprod. 107 (5), 1254–1263.
Wang, W.A., Groenendyk, J., Michalak, M., 2012. Calreticulin signaling in health and disease. Int. J. Biochem. Cell Biol. 44 (6), 842–846.
Wilts, B.D., Vignolini, S., 2019. Living Light: Optics, Ecology and Design Principles of Natural Photonic Structures, vol. 9. The Royal Society, 20180071.
Zhang, L., Martin, A., Perry, M.W., van der Burg, K.R., Matsuoka, Y., Monteiro, A., Reed, R.D., 2017. Genetic basis of melanin pigmentation in butterfly wings. Genetics 205 (4), 1537–1550.
Zhang, Q., Mey, W., Ansorge, J., Starkey, T.A., McDonald, L.T., McNamara, M.E., Jarzembowski, E.A., Wichard, W., Thomson, U., Ren, X., 2018. Fossil scales illuminate the early evolution of lepidopterans and structural colors. Sci. Adv. 4 (4), e1700988.
Zhu, K.Y., Merzendorfer, H., Zhang, W., Zhang, J., Muthukrishnan, S., 2016. Biosynthesis, turnover, and functions of chitin in insects. Annu. Rev. Entomol. 61, 177–196.